Molecules on rails: friction anisotropy and preferential sliding directions of organic nanocrystallites on two-dimensional materials – Electronic Supplementary Information (ESI)

Borislav Vasić,*[a] Igor Stanković,*[b] Aleksandar Matković,*[c] Markus Kratzer,[c] Christian Ganser,‡[c] Radoš Gajić,[a] and Christian Teichert[c]

[a] *Graphene Laboratory of Center for Solid State Physics and New Materials, Institute of Physics Belgrade, University of Belgrade, Pregrevica 118, 11080 Belgrade, Serbia; E-mail: bvasic@ipb.ac.rs*
[b] *Scientific Computing Laboratory, Institute of Physics Belgrade, University of Belgrade, Pregrevica 118, 11080 Belgrade, Serbia; E-mail: igor@ipb.ac.rs*
[c] *Institute of Physics, Montanuniversität Leoben, Franz Josef Strasse 18, 8700 Leoben, Austria; E-mail: aleksandar.matkovic@unileoben.ac.at*
‡ *Present address: Department of Physics, Nagoya University, Furo-cho, Chikusa-ku, Nagoya, Aichi, 464-8602, Japan*

1 Epitaxial relations and lattice registries between 6P and Gr/hBN

Considering β-phase structure of 6P (Baker structure) and known contact planes of 6P with Gr $(11\bar{1})$ and hBN $(\bar{6}29)$, it is possible to express a transformation matrix that connects unit cell vectors of the 2D material substrate and an overlayer of molecules. If considered that the molecular crystal remains in the bulk structure to the very interface, then there is no distinctive registry between the substrate lattice and the deposited lattice, resulting in translational incommensurism. However, molecular crystals can accommodate large strain, and molecules at the surface frequently rearrange to accommodate both intermolecular interactions that drive the formation of the bulk molecular crystal, and interaction with the substrate. As a consequence, the bulk structure of the molecular crystal is not kept at the very interface, and commonly only rotational commensurism is maintained, regardless of the lattice mismatch. An example of the reorganization of the molecules from the interface towards bulk is shown in Fig.1(h) of the main text.

Figures S1 and S2 show schematic representations of the epitaxial relation between 6P bulk structure and Gr/hBN, respectively. Here, shaded red rectangles represent the projection of the molecules on the substrate plane, considering only the molecules that are closest to the substrate and are also closest to have their π networks parallel to the substrate. Filled red circles (placed in the middle of the rectangles that represent the molecules) mark overlayer lattice points, considering only the epitaxial relation of bulk 6P with the substrate.

The unit cell of the substrate is defined by lattice parameters a_1, a_2 (2.46 Å for Gr and 2.50 Å for hBN), and the angle $\alpha = 60°$ between them. Unit vectors were fixed to two zigzag directions of the substrate lattices. The overlayer of 6P, considering the appropriate contact plane, is defined by lattice parameters b_1, b_2, and the angle between them β. The longer lattice parameter was selected as b_1, and chosen as close as possible to being parallel with respect to the long molecular axis direction (LMA). The shorter lattice parameter of 6P overlayer (b_2) was chosen to be exactly in the long needle axis (LNA) direction. The relative orientation of the two lattices is defined with an angle θ taken from a_1 to b_1. All the angles are considered with a plus sign if taken in a clockwise direction. In the case of 6P/Gr interface (Fig. S1), considering $(11\bar{1})$ and $(1\overline{11})$ as the contact planes of 6P, $b_1 = 26.4$ Å, $b_2 = 9.4$ Å, and $\beta = \pm 74°$ were used, where positive angle β was taken for the right-handed case of the chiral pair. Further, $\theta = +11°$, and θ = -71° were considered for right- and left-handed cases of the chiral pair of crystallites. In the case of 6P/hBN interface (Fig. S2), considering $(\bar{6}29)$ and $(\overline{62}9)$ as the contact planes of 6P, $b_1 = 26.9$ Å, $b_2 = 18.6$ Å, and $\beta = \pm 95.4°$ were used, where the positive angle β was taken for the right-handed case of the chiral pair. Similar as in the case of 6P/Gr, angles that define relative orientation between the two lattices, θ = -41.6°, and θ = -18.4° were considered for right- and left-handed cases of the chiral pair of 6P crystallites on hBN.

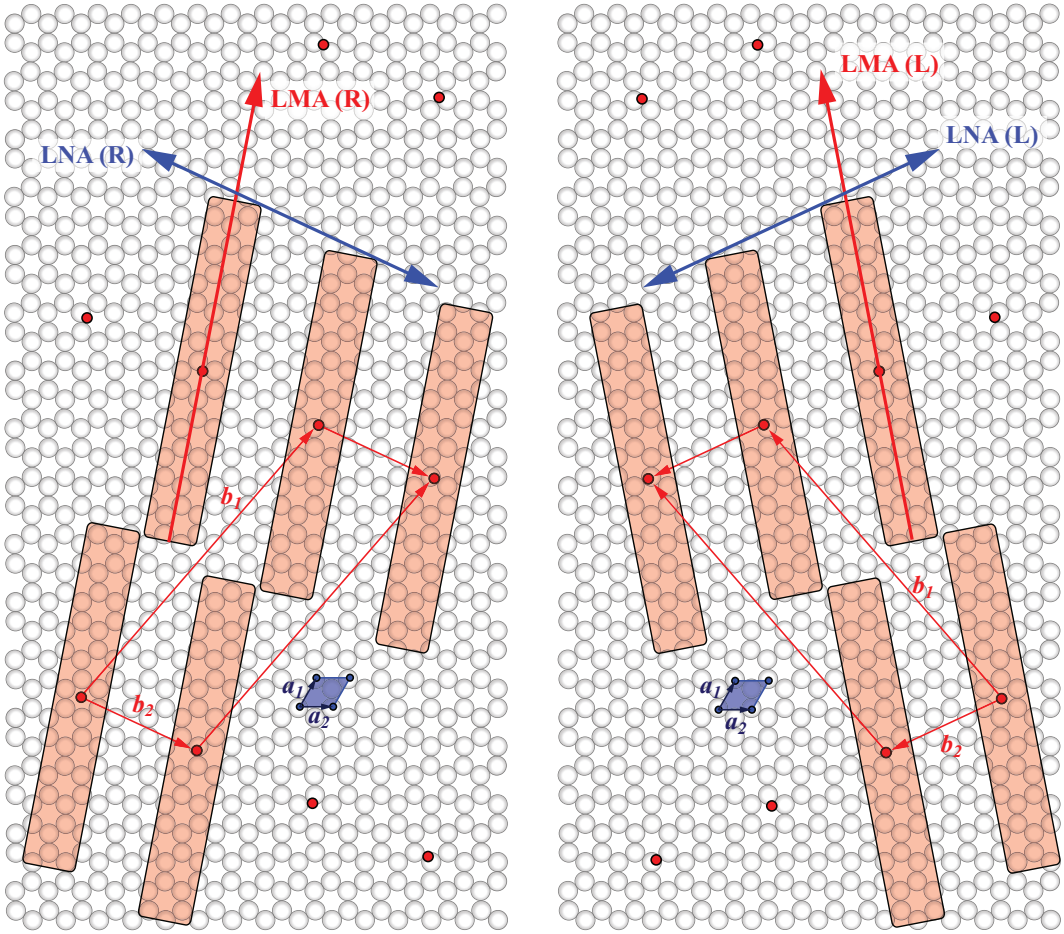

$$\begin{bmatrix} 9.3 & 2.4 \\ -1.9 & 4.4 \end{bmatrix} \qquad \begin{bmatrix} 9.3 & -11.7 \\ -1.9 & -2.5 \end{bmatrix}$$

Figure S1: Schematic representation of 6P/Gr epitaxial relation considering $(11\bar{1})$ or the right-handed crystallites in the right panel, and $(1\bar{1}1)$ or the left-handed crystallites in the left panel. Below each panel, an approximate for the transformation matrix that connects unit cell vectors of the 2D material substrate and an overlayer of molecules is given.

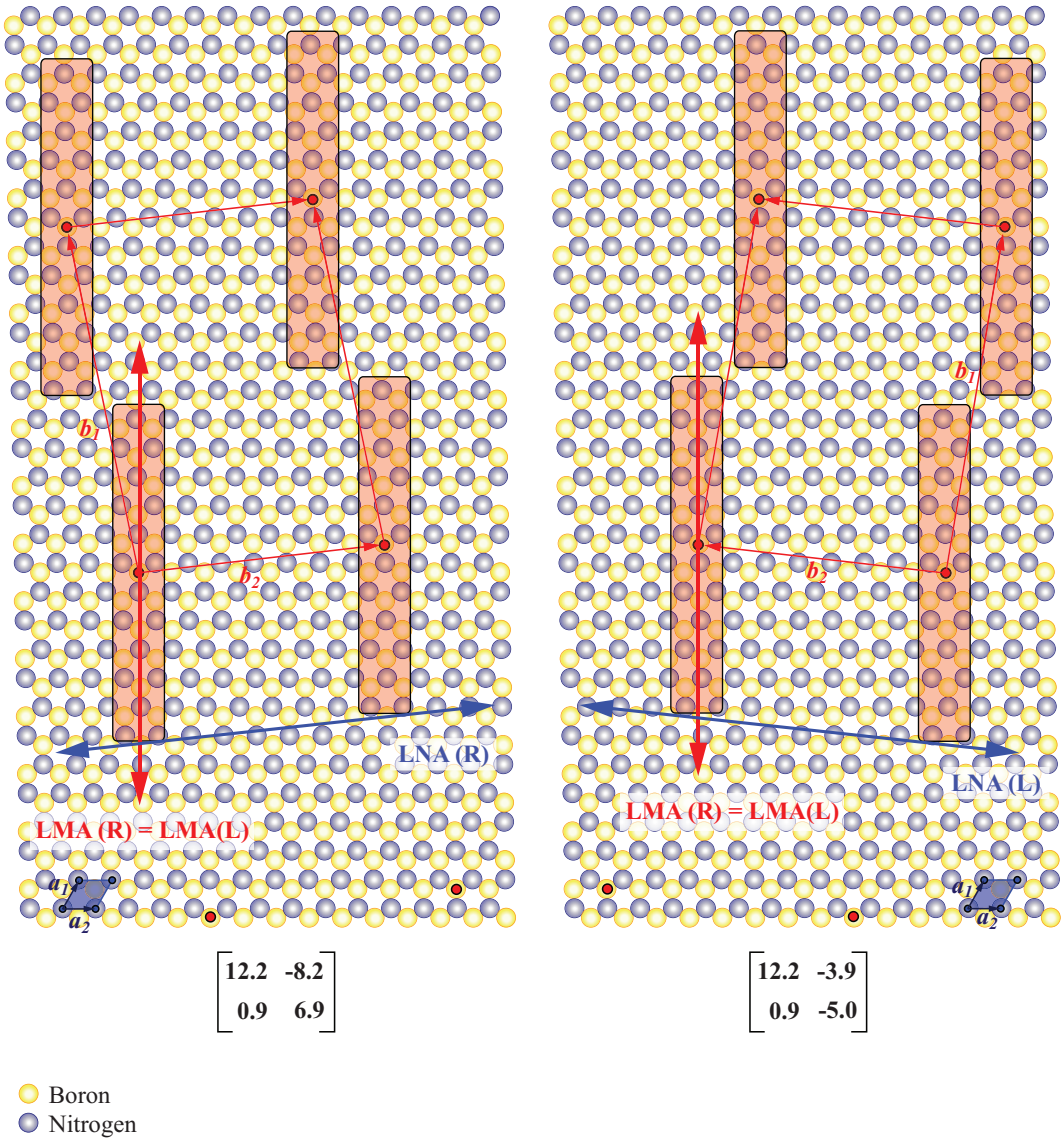

Figure S2: Schematic representation of 6P/hBN epitaxial relation considering $(\bar{6}29)$ or the right-handed crystallites in the right panel, and $(6\bar{2}9)$ or the left-handed crystallites in the left panel. Below each panel, an approximate for the transformation matrix that connects unit cell vectors of the 2D material substrate and an overlayer of molecules is given. Boron atoms are labeled as yellow circles, while nitrogen atoms are labeled as gray circles, and the unit vectors of the substrate are chosen to connect centers of the neighbouring nitrogen atoms.

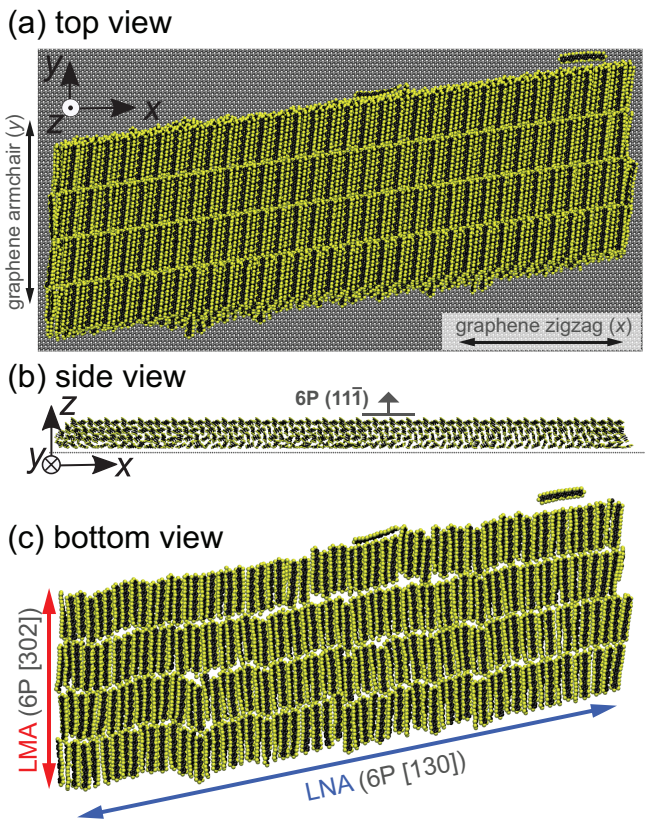

Figure S3: Snapshots of (a) top, (b) side, and (c) bottom view of a particular simulation run demonstrating the MD simulation setup. Gr is shown in gray. C and H atoms within the molecules are represented with black and yellow colors, whereas LMA and LNA are depicted by arrows.

2 MD simulation setup

MD simulation setup for a needle fragment composed of $64 \times 4 \times 4$ 6P molecules is depicted in Figs. S3(a-c) for top, side, and bottom view, respectively. LMA and LNA are denoted in parts (a) and (c), with LMA oriented along y-axis, while the angle between LMA and LNA is around 74°. Top 6P molecules in Fig. S3(a), are fixed, while the rest of the system is thermalized and free to move. The contact plane of the top, fixed layer is (11$\bar{1}$). It is used to impose an external velocity and/or a rotation during movements of the whole needle. The side view depicted in Fig. S3(b) shows the transition of molecules at the bottom layer in contact with Gr in part (c) to bulk herringbone structure with (11$\bar{1}$) contact plane in part (a). Please note that Fig. S1 shows the structure of the needle after one full rotation, and thus there is a slight miss-mach of LMAs between the molecules in the bottom and the top row of the model crystallite.

3 Fabrication of a short 6P needle by AFM based cutting

After the growth of 6P needles, appropriate areas for AFM manipulations were selected as exemplified in Fig. S4(a) for 6P needles on hBN substrate. The area contains two long needles, labeled with LN_1 and LN_2 which are along two preferential growth directions, D_1

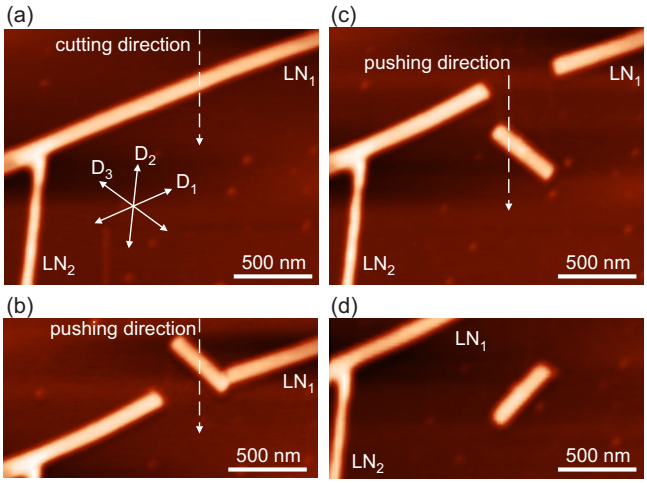

Figure S4: Topographic AFM images during the fabrication of a short needle: (a) initial topography, (b) after the cutting, (c) and (d) after the pushing. The preferential growth directions are denoted in part (a) with $D_1 - D_3$. The dashed arrow in part (b) denotes the direction for AFM cutting in contact mode, whereas the dashed arrows in parts (b) and (c) indicate the pushing directions. z scale in the images is 15 nm.

and D_2, respectively. They are separated from each other by 120°. According to the hBN symmetry, the third preferential growth direction marked with D_3 is depicted in Fig. S4(a). AFM in contact mode was then used to cut a short needle from LN_1. After the initial cutting, the newly formed short needle was pushed by the AFM tip several times as is indicated in Figs. S4(b) and S4(c), and finally placed on a needle-free hBN area depicted in Fig. S4(d), which is appropriate for next AFM manipulations. The same procedure was applied to needles grown on Gr substrate in order to fabricate corresponding 6P needle segments.

4 Rotations across registry state

From around 100 AFM manipulations of 6P needle fragments on Gr, the needle rotation across the registry state defined with the direction D_2 was observed for around 20 times. Three such cases were preented in the main manuscript, whereas further cases are depicted in Fig. S5 (cases where all lateral force levels could not be measured were excluded from the analysis). In all cases, we observed double peaks in the lateral force profiles (domains containing these peaks are highlighted by yellow colour in Fig. S5), while in the cases for pure rotations (without translation), the angular separation between the peaks was around 20°.

5 Supplementary movies

Supplementary movie 1 (2) presents a sequence of all AFM tapping mode images recorded after all AFM manipulation steps on hBN (Gr). Supplementary movie 3 presents a sequence of snapshots of the bottom layer of 6P needle fragment on Gr obtained by MD simulations during the needle rotation.

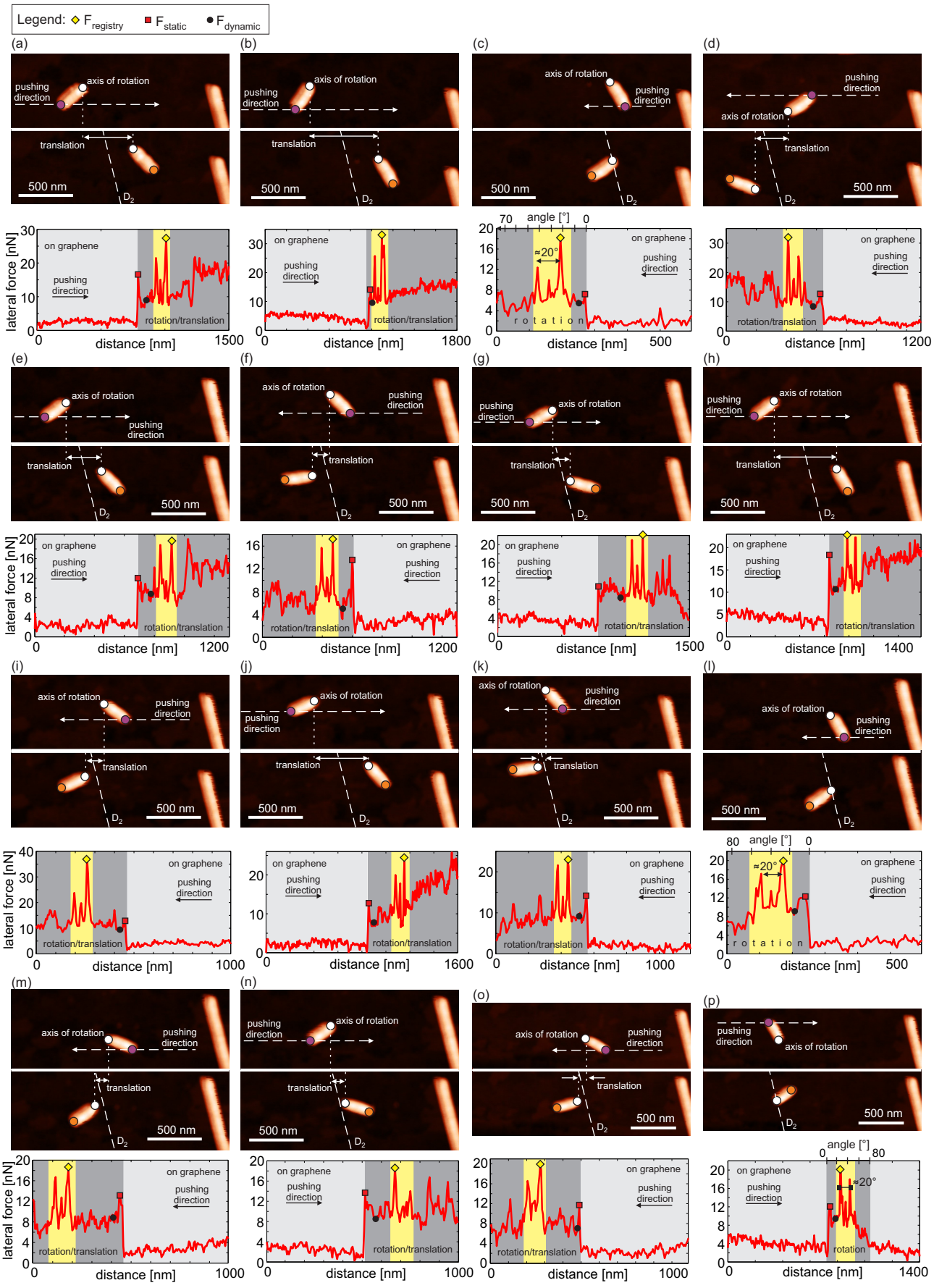

Figure S5: Figure caption continued on the next page.

Figure S5: Rotations across the registry state determined by direction D_2 on Gr. All parts (a-p) contain topographic images before AFM manipulation (top row), topographic images after the manipulations (middle row), and lateral force profiles during the AFM manipulations (bottom row). z scale in the images is 10 nm. The yellow domains in lateral force profiles emphasize double peaks when the needle is rotated across the registry state. In parts (c), (l), and (p), the angle axis was approximately determined showing that the angular separation between two peaks is around 20°.